Supporting Information

Gallium-Indium Nanoparticles as Phase Change Material Additives for Next-Generation Thermal Fluids

Jacob Mingear, Zachary Farrell, Darren Hartl, Christopher Tabor*

Additional Comments on Particle Means, Standards of Deviation, and Distribution Metrics

The Ga-In nanoparticles had a narrower distribution of particle sizes as a function of sonication time, though these distributions were log-normal, as is typical for particles produced via top-down methods [29][33]. Since this study directly involved relating these particle sizes to thermal measurements, a meaningful descriptor of such distributions and their expected relationship to nanoparticle physical properties were needed. In terms of number distribution, arithmetic means (AM) are not well suited for log-normal distributions, while geometric means (GM) match closer to the peak of the distribution, as seen in **Figure S1**. The standard deviation (STD) for GM is also a much better descriptor for log-normal distributions [34] than AM, and as easy to calculate**.** Further, the AM STD is on the order of the AM itself, whereas the GM STD is much more meaningful indicator. **Figure S2A** and **S2B** compares the means and STDs for AM and GM as a function of sonication time.
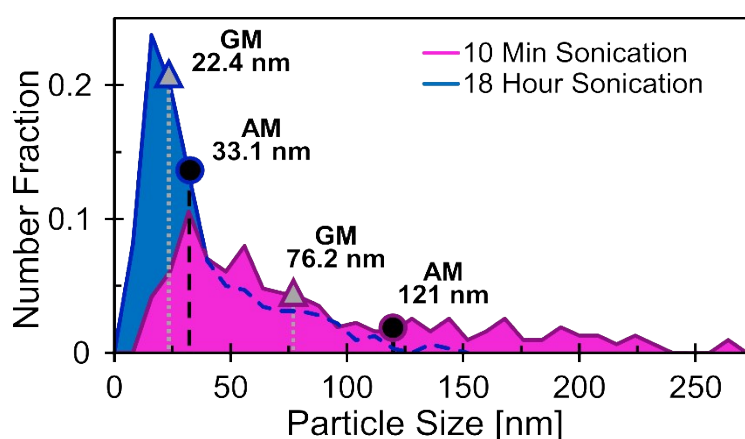
Figure S1. A comparison of Arithmetic Mean (AM) and Geometric Mean (GM) for the number fraction distribution of a system of nanoparticles. GM is a better descriptor of such log-normal distributions.
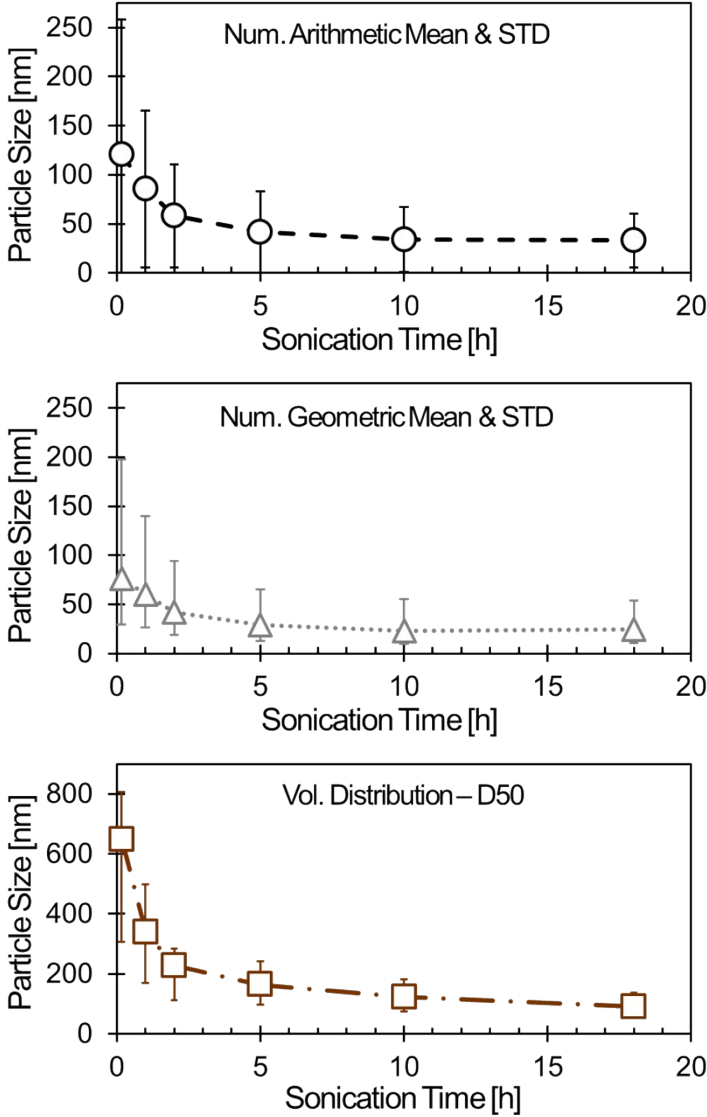

Figure S2. Three metrics to describe the particle systems in the work as a function of sonication time. (A) The number fraction AM with 1 AM-STD, (B) number fraction GM with 1 GM-STD, (C) volume fraction D_V-50 value with D_V-16 and D_V-84.

However, as the overall goal is to understand the thermal effects of such distribution, additional consideration is required. Currently, the distributions have been described in terms of their

2

number fraction. When considering each particle's volume fraction against the whole system, the many smaller particles have very little consequence to the physical thermal effects. Further, when calculated in terms of volume fraction, the cumulative distribution value is a sufficient descriptor for these log-normal distributions. Thus, the D_V50 values and related D_V16 and D_V84 are displayed in **Figure 2SC**. **Figure S3** compares the number and volume distribution curves for the same 18 h sonication sample; note how the D_V50 matches well with the volume fraction peak. Finally, **Figure S4** shows the equivalent distributions from Figure S1, though in terms of volume distribution. For very wide log-normal volume distribution, (e.g., that found in the 10 min sonication samples in Figure S4), the D_V50 is not as sufficient as an indicator, which is why the majority of reported data in this work consisted of 18 h sonication samples. **Figure S5** further shows the differences between number and volume distributions.
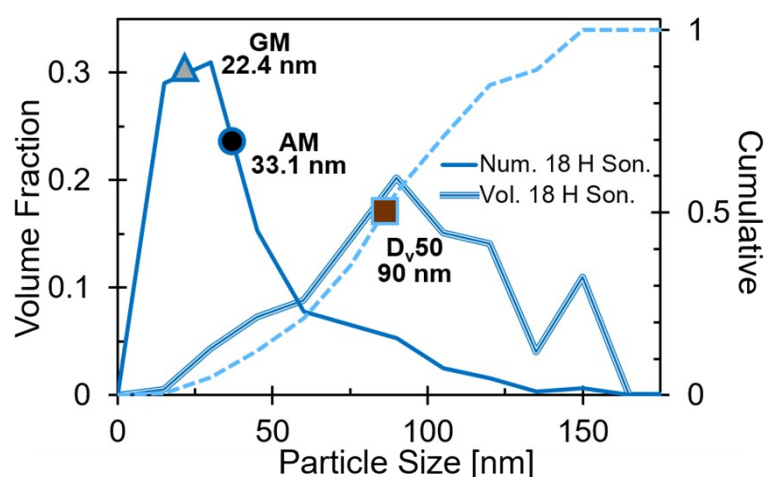

Figure S3. A comparison of AM, GM, and D_V-50 with respect to their appropriate number or volume fraction distribution. Thermal effects are better represented by a volume fraction.
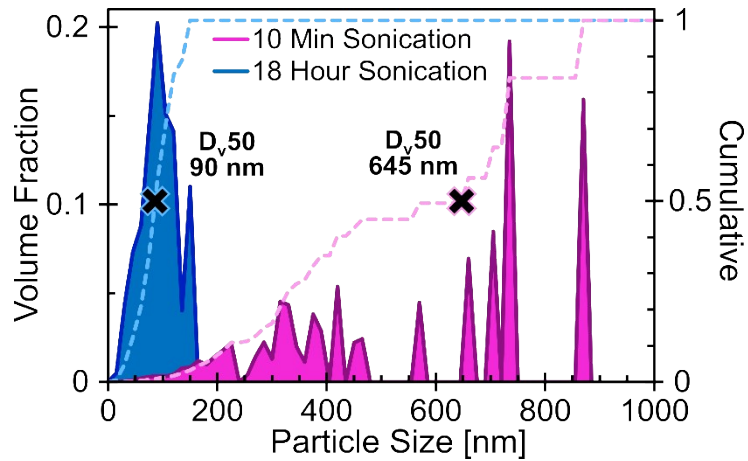
Figure S4. The equivalent distributions from Figure S1 in terms of volume distribution. Further, this shows that wide distributions such as those found in 10 min sonication samples, still are not described well.
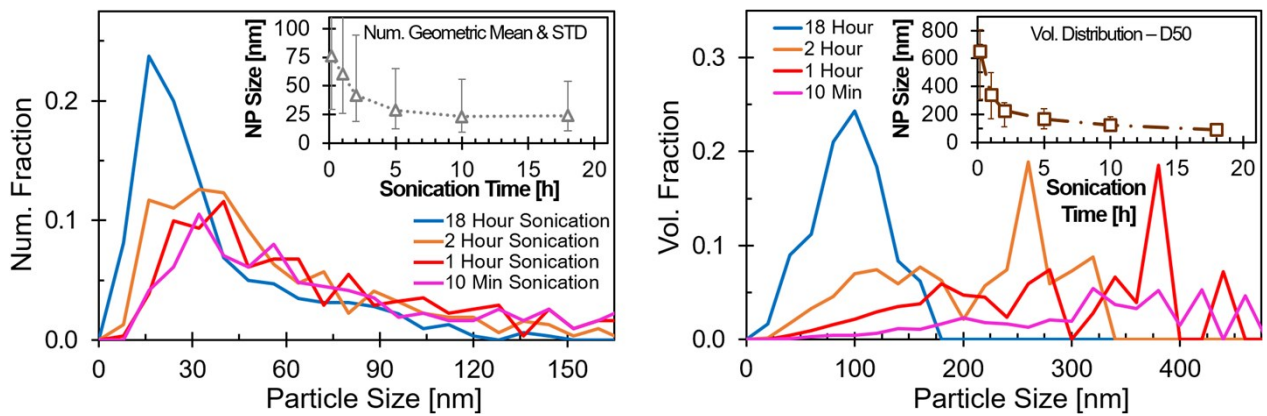

Figure S5. A comparison of number distribution (bin of 8) and volume distribution (bin of 20) of Ga-In nanoparticles. The volume D_V-50 is significantly higher than the geometric mean, even more so for wider distributions. For thermal measurements, the volume distribution is a significantly better indicator for expected measurements.

Additional Comments on Methods:

Ga-In PCM Nanoslurry Production: A Ga-In PCM nanoslurry contains Ga-In nanoparticles in a thermal fluid, i.e. usually AR-200 silicone oil in this work. Nanoslurries of Fomblin® Y,

polyethylene glycol ($M_w = 200$), and paraffin oil as the thermal fluid were produced and showed similar results to that of AR-200.

Particle Size Characterization: Nanoparticle sizes and size distributions were measured similarly to the procedure of Yamaguchi et al.[29] An energy dispersive x-ray spectroscope (EDS) was used for chemical verification. FIJI ImageJ software was used to facilitate particle counting using its differential gradient image processing function to more accurately identify particle edges.

Thermal Analysis: DSC measurements for the Ga-In nanoparticle slurries and Ga-In bulk underwent multiple sequential and non-sequential cycles and showed consistent onsets of transformation. A significant selection of samples underwent DSC testing with temperature ramp rates of 1, 2, 5, 10 °C/min to verify similar responses.

Despite the nanoparticles consisting of largely gallium, which is known to embrittle and alloy with aluminum, no reaction between the nanoparticle samples and the pan was observed, even after 110°C temperature cycling. This is likely due to the effects of a protective gallium-oxide shell, low vol.% of particles, and/or sufficient wetting by the thermal fluid to the pan.

Rheological Analysis: Higher shear rates could not be obtained due to fluid ejection, a limitation of parallel-plate rheology. Measurements utilizing bob-and-cup geometry could overcome fluid ejection higher shear rate analysis, but such device geometry was not available during the testing described in this manuscript.

Comments on the Effects of Composition on Nanoparticle Production

The initial droplet of Ga-In alloy could be varied in composition before nanoparticles were processed using ultrasonication. Composition was varied between 0, 5, 10, 15.9, and the eutectic 21.4 wt.% In, for 10°C while limited additional samples were produced above 60°C for 30, 40, 50, and 60 wt.% In. The higher temperature during sonication ensured that the Ga-In droplet was fully liquid, otherwise eutectic composition could separate from In-rich

particulates and create a variety of nanoparticle compositions in a single sample. During sonication, the composition range between 0 - 30 wt.% In produced particles within seconds of probe initiation, indicted by the solution turning black and opaque. Compositions of 40 wt.% In seemed to require much longer time periods to create nanoparticles as there was no immediate indication of particle creation; eventual particles were created but a significant mass of the initial droplet remained. 50 and 60 wt.% In did not result in any indication of particle creation even after 1 h at a 25% increase in the standard sonication power; no discoloration of the solution nor a change in the initial liquid metal droplet was observed.

Bulk Liquid Metal Thermal Measurements

To better understand the DSC data from the Ga-In nanoparticles, bulk Ga-In droplets, 2-4 mm in diameter, were measured in graphite loose-lid DSC pans. Seen in **Figure S6**, the heating curves matched the known phase diagram for the (αGa)-In system compiled by Anderson and Ansara [43]. From the cooling curves, significant undercooling occurred until full crystallization around -25°C to -30°C. Further, a small exothermic transition on the cooling curve was detected at a few degrees below the In liquidus transition temperatures which is believed to be the onset of In nucleation (not shown). Supporting this claim: the enthalpy associated with this minor transition increases as wt.% In increases, and this transition is not detected on samples with less than <10 wt.% In.
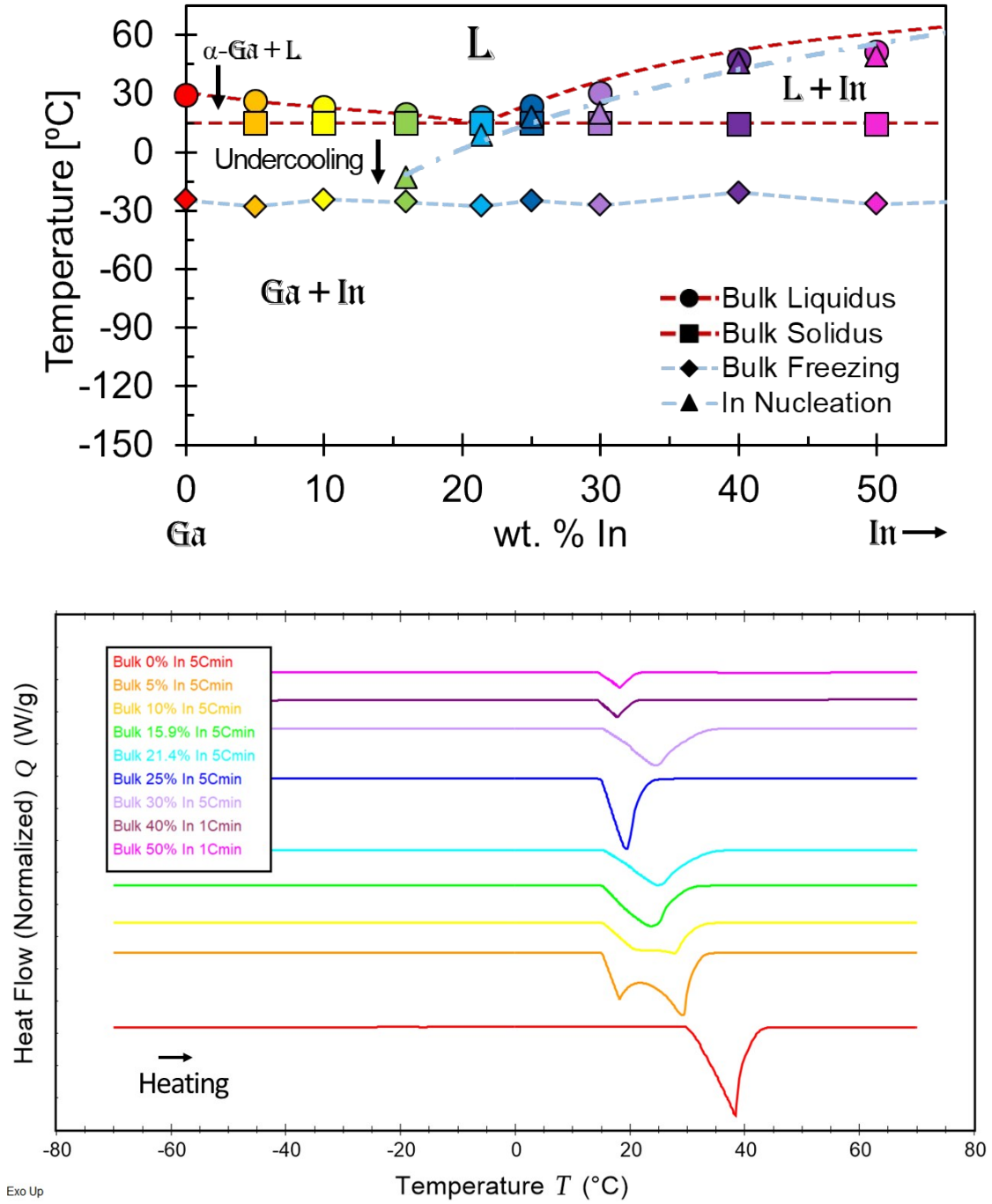
Figure S6. A Bulk thermal of compiled into a Ga-In phase diagram. **B** The heating curves

match the (αGa)-In phase diagram.

Equation for Core Composition Change as a Function of Particle Diameter

Using **Equation 1**, one can estimate the core composition of the particle after the oxide shell

formation.

$$N_{In,core} = 1 - \frac{N_{Ga}d^3 - 0.4(d^3 - (d - 2t)^3)}{N_{Ga}d^3 - 0.4(d^3 - (d - 2t)^3) + N_{In}d^3}$$ (1);

where d is the particle diameter, t is the oxide thickness, N is the initial atomic fraction, and the 0.4 stems from the atomic fraction of Ga in Ga_2O_3. Shown in **Figure 1C**, the oxide can increase the overall indium content in the core of the particle and is more pronounced for smaller particles.

Equations for Thermal Properties of the Liquid Metal PCM Nanoslurries

The thermal conductivity of diluted particle dispersions in a media can be evaluated using Maxwell-Eucken 's relationship [8]:

$$\lambda_{system} = \lambda_f \frac{2 + \frac{\lambda_p}{\lambda_f} + 2\phi\left(\frac{\lambda_p}{\lambda_f} - 1\right)}{2 + \frac{\lambda_p}{\lambda_f} - \phi\left(\frac{\lambda_p}{\lambda_f} - 1\right)}$$ (2) ;

where ϕ is the volume fraction of the particles while λ_f and λ_p are the thermal conductivity of the fluid and particle, respectively.

With the linear rule of mixtures, one can estimate the specific heat capacity at a single temperature with any wt. % of nanoparticles:

$c_{system} = w_i c_p + (1 - w_i)c_f$ (3);

where c_p is the isobaric mass heat capacity of the nanoparticles and w_i is the weight fraction of the nanoparticles. To keep terms in volume fraction,

$$w_i = \frac{\phi\rho_p}{\phi\rho_p + (1 - \phi)\rho_f}$$ (4) ;

Thermal diffusivity combines the previous discussed heat capacity and thermal conductivity, while also including its relation to density. Thus, one can calculate the thermal diffusivity, α, by the simple relationship:

8

$$\alpha = \frac{\lambda}{\rho c} \ (5)$$

where ρ is density which changes value for each volume fraction with relation to:

$$\rho_{system} = \left(\frac{w_i}{\rho_{particles}} + \frac{1-w_i}{\rho_{fluid}}\right)^{-1} (6)$$

Nanoscale Melting Point Depression

It is believed that some type of melting point depression effect attributed to the high surface-to-volume ratio of these systems is occurring compared to their bulk counterparts. Approximations of such melting point depression were calculated for pure αGa phase using three thermodynamic models known as the Liquid Shell Model (LSM), Homogenous Melting Model (HMM), and the Liquid Nucleation and Growth Model (LNG) [51]–[53]. These models were based on the pure gallium forming the αGa phase due to data availability, though our data herein suggesting that a non-αGa phase was forming. These models are plotted in **Figure 3B** based on **Equations S7** and **S8** below.

$$T_m(d) \approx T_{m,\infty}\left(1 - \frac{4\alpha}{H_{f,\infty}\rho_s d}\right) (7)$$

$$\alpha = \begin{cases} \dfrac{\dfrac{\sigma_{sl}}{r_o} + \sigma_{lv}\left(1 - \dfrac{\rho_s}{\rho_l}\right)}{1 - \dfrac{r_o}{r}} & LSM \ (8a) \\[2em] \sigma_{sv} - \sigma_{lv}\left(\dfrac{\rho_s}{\rho_l}\right)^{2/3} & HMM \ (8b) \\[2em] \sigma_{sl} + \dfrac{3}{2}\left(\sigma_{sv} - \sigma_{lv}\left(\dfrac{\rho_s}{\rho_l}\right)\right) & LNG \ (8c) \end{cases}$$

Though the arithmetic mean particle size of this work was 33 ± 27 nm based on the number distribution, the thermal data should be associated volume distribution and thus the D_V50 value of 90 nm is more appropriate. At a value of 90 nm, there should be a detectable melting point depression up to a maximum change of 15°C, which may explain the observed

melting point of -31°C found for pure Ga, which does not match the established δGa (T_m = -19°C) or εGa (T_m = -28°C) phases.